Food Control 144 (2023) 109351

Contents lists available at ScienceDirect

Food Control

journal homepage: www.elsevier.com/locate/foodcont

Single-drop technique for lactose prediction in dry milk on metallic surfaces: Comparison of Raman, FT – NIR, and FT – MIR spectral imaging

Vicky Caponigro [a,d,e,*], Federico Marini [b], Amalia G.M. Scannell [c,d], Aoife A. Gowen [a,d]

[a] UCD School of Biosystems and Food Engineering, UCD, Belfield, Dublin, D04 V1W8, Ireland
[b] Dipartimento di Chimica, Sapienza Università di Roma, Piazzale Aldo Moro 5, Rome, Italy
[c] UCD School of Agriculture and Food Science, UCD, Belfield, Dublin, D04 V1W8, Ireland
[d] UCD Institute of Food and Health, UCD, Belfield, Dublin, D04 V1W8, Ireland
[e] Department of Pharmacy, University of Salerno, Via Giovanni Paolo II, 132, 84084 Fisciano, Italy

ARTICLE INFO

Chemical compounds studied in this article:
Lactose (PubChem CID: 62223)

Keywords:
Milk
Lactose
Raman
FT
NIR
FT-MIR
Spectral
Hyperspectral
Imaging
Aluminium
Stainless steel
PLS

ABSTRACT

This study applies the single drop techniques to compare the efficacy of Raman, FT – NIR, and FT-MIR spectral imaging to quantify lactose concentration in dried whole milk on different metallic surfaces. Drying the samples avoids degradation problems such as water evaporation or oil degradation and scattering due to micelles. Spectral imaging techniques minimise sampling issues while also describing the sample spatial variation. The mean spectra of pre-processed images were used to build PLS regression models to predict lactose concentration. Raman, FT – NIR (5600–3730 cm^{-1}), FT–MIR (3533–600 cm^{-1}) models and the model obtained using the fusion of the three ranges were built independently and compared. This study confirms that is possible to quantify lactose rapidly using spectral imaging without adding standard references: the minimum RMSEP = 2.8 mg/mL (R^2 = 0.98) was achieved with FT – MIR spectral imaging.

1. Introduction

Milk, an emulsion with different components (i.e., fats, water, proteins, and carbohydrates), is a complex matrix. Lactose intolerance is a common genetic condition that has increased the demand for "lactose-free" or "low lactose concentration" products and, in general, the requirement for products with controlled lactose concentration. To control milk quality and comply with labelling legislation, dairy industries need a cost-effective, accurate, sensitive, and robust lactose quantification method. Standard techniques, such as gravimetry, polarimetry, mid - infrared (MIR) detection, chromatography, and differential pH assay, are currently applied worldwide for lactose determination. A schematic and complete description of them can be found in Gambelli (2017).

Spectroscopic techniques have been investigated for non-destructive analysis of chemical components in several food matrices, for instance for food authentication (Biancolillo et al., 2020; Li Vigni et al., 2020), assessment of food safety (Valand et al., 2020; Wu et al., 2021), determining adulteration, for example in butter (Taylan et al., 2020), or to control packaging degradation (Baskaran & Sathiavelu, 2020). As such, these techniques are gaining traction as a robust quality control tool.

In terms of milk, the mid-infrared region has been extensively investigated as a major tool to quantify milk components (Portnoy & Barbano, 2021). For instance, protein, carbohydrate, and fat content have been quantified in commercial milk from different regions (Italy, Switzerland, and Spain) comparing the performances of a portable and a benchtop ATR – MIR (Gorla et al., 2020). In a recent study, lactose, protein, fats and total solids contents in raw cow and camel milk have been analysed using both near-infrared and mid-infrared spectroscopy. A correlation between the two types of milk has been assessed (Mohamed et al., 2021).

Focusing on lactose, mid-infrared spectroscopy using the ATR

* Corresponding author. UCD School of Biosystems and Food Engineering, UCD, Belfield, Dublin, D04 V1W8, Ireland.
E-mail addresses: vicky.caponigro@ucdconnect.ie (V. Caponigro), federico.marini@uniroma1.it (F. Marini), amalia.scannell@ucd.ie (A.G.M. Scannell), aoife.gowen@ucd.ie (A.A. Gowen).

https://doi.org/10.1016/j.foodcont.2022.109351
Received 20 May 2022; Received in revised form 20 August 2022; Accepted 29 August 2022
Available online 3 September 2022

modality has been successfully applied to discriminate between regular and lactose-free cow milk. In addition, the range 935–1200 cm^{-1} was found has the most suitable for lactose quantification (Pinto et al., 2021).

In addition, lactose has been quantified using Raman spectroscopy in combination with crystal violet as an internal standard by Li et al. (2015). Phenylalanine and crystal violet internal standards for lactose quantification in dried milk have been compared by Vaskova and Buckova (2016). More generally, a recent review summarises the application of Raman spectroscopy in the dairy field (He et al., 2019).

Analysis of the aqueous phase in a milk emulsion can be challenging, as water has a strong signal in the Infrared region which can cover some desirable information. Also, water can represent a problem for analyses over a prolonged time period as evaporation changes the sample and consequently its vibrational spectrum. As reported by Lynch, Barbano, Schweisthal, and Fleming (2006), Mohamed et al. (2021) and Pinto et al. (2021) sample inhomogeneity, i.e., the casein micelles and fat globule structure can represent a problem during the analysis. In fact, the tridimensional structure may induce light scattering, affecting the spectroscopic analysis (Cattaneo et al., 2009). In addition, the experimental conditions (i.e., temperature, pH, agitation, etc.) can change the micelles' structure and so the sample homogeneity and cause fat deterioration (Holt et al., 2013; McMahon & Oommen, 2008). Pinto et al. (2021) propose the use of spectral pre-processing, such as Multiplicative Scatter Correction (MSC), as a solution. In another paper, to avoid fat deterioration and sample inhomogeneity, milk samples were maintained at 41 °C (Lynch et al., 2006). In addition, the presence of water affects the signal-to-noise ratio (S/N) in Raman spectra: in particular, the impact on the spectral signal, and, consequently, on model quality, becomes more and more relevant with increasing spectral resolution. Mazurek et al. (2015) solved this problem using chemometrics tools like Fast Fourier transform (FFT) filter to remove the noise from Raman spectra and MVN algorithm to normalise the spectra. However, the error for the test set in Mazurek et al. (2015) was higher than in the study of Pinto et al. (2021).

To overcome these problems, a single dry drop approach is investigated in this study as a potential solution. The milk samples have been analysed after 48h as the maximum drying time point. In order to investigate possible sample inhomogeneity during the drying process, spectral imaging techniques have been used. In fact, previous research has indicated that spectral imaging is superior to traditional point scan spectroscopy as it alleviates sampling problems, providing a suitable method to ensure that the multiple point approach is representative of the entire sample (Alves da Rocha et al., 2015; Tan et al., 2017).

In addition, the applications of spectral imaging in the dairy field have been extensively reviewed and discussed in the chapter *"Spectral Imaging for Dairy Products"* (Gowen et al., 2020). Recent research has demonstrated the ability of spectral imaging, specifically Raman and FT – IR, to distinguish different dairy products based on fats and carbohydrates content (Caponigro et al., 2019)

This study focuses on the spectral imaging analysis of a single dry whole milk drop with varying lactose concentrations applied on surfaces related to dairy production, i.e., stainless steel AISI - 304 and AISI - 316 and aluminium. These surfaces can be washed and sterilised as the industrial process requires. In order to study the lactose distribution over the drop and an eventual sample inhomogeneity, spectral imaging has been preferred to traditional point scan spectroscopy to accomplish the experimental goal: quantifying lactose in dry milk. The study aimed to optimise image pre-processing and create robust models of micro - Raman and FT – IR spectral images of lactose drops using independent Partial Least Squares regression (PLS) models to define the best prediction model.

2. Material and methods

2.1. Sample preparation

Whole milk (Avonmore Ltd, Avonmore, Ireland) used for this study was purchased at local shops. Two series of samples, using selected lactose concentrations, were prepared by adding both deionised water and standard lactose (Lactose monohydrate; CAS number 10039 - 26–6: Merck KGaA, Frankfurter Strasse 250, 64293 Darmstadt, Germany) solution (72 mg/mL). The lactose concentrations tested are 72 mg/mL, 62 mg/mL, 60 mg/mL, 58 mg/mL, 48 mg/mL, 29 mg/mL, 24 mg/mL, 19 mg/mL. The products were stored in 3 mL test tubes in a fridge at 6 °C. Two tubes for each sample were removed from the fridge, one to measure the temperature and the other to pour the milk on the surface. 1 drop of 15 μL for each mixture was applied onto aluminium, stainless steel AISI 304 (18% chromium and 10% of nickel) and AISI 316 slides (17% chromium, 12% nickel and 2.5% molybdenum) (37 mm × 25 mm × 1 mm) [purchased from Rice Metals (Cornwall, United Kingdom)] after the sample reached room temperature (20 °C).

The metallic surfaces were supplied covered with protective tape. They were washed with a (1: 1 v/v) solution of ethanol (99%, Absolute, Extra Pure, SLR; CAS Number: 64 - 17–5: Fisher Scientific, Dublin, Ireland), and acetone (HPLC grade; CAS Number: 67–64 - 1: Fisher Scientific, Dublin, Ireland), to remove any traces of glue. Each slide was immersed for 10 min in the acetone/ethanol solution and was then rinsed for 5 min with deionised (DI) water sourced from a Thermo Scientific™ Barnstead™ Smart2Pure™ water purification system (producing Type I ASTM water, with a resistivity of 18.2 MΩ cm at 24.7 °C). Each sample was dried at room temperature (about 20 °C), for 48 h prior to analysis. Three independent repetitions were prepared for each combination. In order to obtain independent repetitions, different milk batches were bought in different stores and different periods (one per week, over three weeks). Lactose solution was freshly prepared for each experiment. In total, 72 images per instrument have been collected (8 concentrations x 3 surfaces x 3 independent repetitions).

2.2. Spectral imaging system and data collection

2.2.1. Raman spectral image measurement

Each sample was scanned using InVia micro - Raman spectroscopy system from Renishaw that includes Leica DM2500 M microscope and NIR - enhanced deep depletion CCD array (1024 × 256 pixels). Each image was recorded using a 785 nm laser (306 mW) excitation, set to 50% power for 5 s per spectrum. The total range scanned was: 4000 - 190 cm^{-1} using two ranges (range 1: 2410 - 190 cm^{-1} and range 2: 4000–2360 cm^{-1}) with an average spectral resolution of 1.8778 cm–1200 spectra were recorded using Leica 50× objective lens (0.75 NA) covering an area of 1.90 × 0.90 mm for each image. Internal silicon was scanned daily to control the instrument calibration. The images were saved in Renishaw WDF format.

2.2.2. FT – IR spectral image measurement

The same sample was analysed with iN10 MX Imaging Microscope (Thermo Ltd) with LN2 Cooled MCTA linear array detector after collecting the Raman spectral image. This system collects the NIR and MIR range simultaneously. The FT – IR reflectance image constituted of 300 spectra, recorded with aperture size of 150 × 150 μm using 150 μm step covering an area of 3.00 × 2.25 mm 16 acquisitions were acquired per pixel in 5 s. The average spectral resolution was 1.928 cm^{-1} for the total range 720–6000 cm^{-1}. A gold spectrum was collected before each image, and it was used as background reference. Each file was transformed in ENVI format from Nicolet Map file format using Omnic Picta software (Thermo Ltd).

2.3. Data analysis

2.3.1. Data pre-processing

Data processing was carried out using Matlab R2019a (The MathWorks Inc, Natick, MA, USA). Data analysis was performed with a combination of in-house developed code and PLS toolbox 8.8 (R8.8.1: Eigenvector Research Inc, Manson, WA, USA).

Firstly, saturated pixels were masked out from the Raman images. Cosmic rays were removed from the Raman spectra using an in-house function that recognises the anomalous spikes comparing all the peaks over all spectra and evaluating the peak width. Cosmic spikes were substituted with a linear interpolation of the 5 neighbouring wavenumber baseline (Piqueras et al., 2014). The two spectral ranges were reduced to range 1: 3600–2500 cm^{-1} and range 2: 2000–230 cm^{-1} to maximise the chemical information and reduce the noise. Penalized Asymmetric Least Squares (AsLS) smoothing was applied to Raman spectra in the separated ranges to correct the baseline and remove the fluorescence interference. The two ranges were corrected using the following parameters: $p = 0.00001$, $\lambda = 10^4$ for range 1 and $p = 0.0001$, $\lambda = 10^4$, for range 2, respectively, with 50 iterations in both cases (Eilers, 2004). Ultimately, a single spectrum was obtained by concatenating ranges 1 and 2.

iN10 MX Imaging Microscope allowed the simultaneous collection of Near Infrared (NIR) and Mid Infrared (MIR) ranges. These were split into two ranges (NIR: 5600 - 3730 cm^{-1} and MIR: 3533 - 600 cm^{-1}). FT – IR data were collected in reflectance mode. The signal was transformed in pseudo absorbance calculating the logarithm of the reciprocal reflectance value in order to apply the Lambert – Beer's law and underline the peaks. They were pre-processed independently. Two pre-processing methods were applied to the image spectra to improve the PLS model performance reducing the source of noise:

1. Standard Normal Variate (SNV), a common scatter correction tool, especially in NIR spectral imaging (Barnes et al., 1989).
2. Savitzy - Golay 1st derivative (SV1) (window size = 15 and polynomial order = 3), removes the different effect on the baseline: the first derivative is useful for horizontal baseline (Savitzky & Golay, 1964).

The spectra were analysed independently for the NIR and MIR range. The spectroscopic signal of NIR overtones is 10–100 times weaker than MIR molecular vibrations. Consequently, to facilitate comparison between the ranges, the two blocks were scaled by their respective Frobenius' norm. Spectra pre – processed by SNV are shown to define the lactose signal in section *2.1. Comparison of milk and lactose spectroscopic signal.* SV1 spectra were used to build the PLS model.

The mean spectrum of each spectral image for all modalities (Raman, FT – MIR and FT – NIR) was calculated after pre - processing. These spectra were analysed using Principal Component Analysis (PCA) and were split into calibration and test sets using the Kennard - Stone method (Kennard & Stone, 1969).

A second type of pre –processing, External Parameter Orthogonalization (EPO), was applied to the mean spectra before building a Partial Least Squares regression (PLS) model on each block (Raman, FT – MIR and FT – NIR). EPO was applied in order to remove the effects due to the different surfaces. EPO was built using the calibration set and it was applied to the test set. Data with EPO correction were then used to build the PLS model (Roger et al., 2003).

2.3.2. Principal component analysis and Kennard - Stone algorithm

In order to split the data in calibration and test set, the Kennard - Stone algorithm was applied to Raman, FT – MIR and FT – NIR data. (Kennard & Stone, 1969). The baseline was removed from Raman data using AsLS and FT – NIR and FT – MIR spectra were corrected by SNV and SV1 as explained above. Three principal component analysis (PCA) models were calculated independently on the pre – processed mean centered data (Jollife & Cadima, 2016). To facilitate comparison of the PLS models from the different spectral modalities, it was necessary to have the same calibration and test set. Consequently, the scores values have been concatenated after being scaled by their respective Frobenius' norm. The obtained block was used as input for the Kennard –Stone algorithm in order to split the data into calibration and test sets. The calibration set covers 70% of the data (51 images) and the remaining 30% (21 images) was assigned to the test set.

2.3.3. Partial least square regression

Partial Least Squares regression models (PLS) were built independently and compared for Raman, FT – NIR and FT – MIR. In a second step, the blocks were fused after being scaled by their respective Frobenius' norm and used to build a fourth PLS model. Random cross-validation was performed on the calibration set using 6 cancellation groups and 20 iterations in order to select the optimal number of latent variables (nLVs). The nLVs are chosen to minimise the Root Mean Square Error of Cross – Validation (RMSECV) within the first 20 LVs. Lactose concentration in the test set was predicted using the built models. Calibration and test mean spectra were mean centered before building the PLS models. Each selected model was evaluated using Root Mean Square Error of Calibration (RMSEC), Root Mean Square Error of Cross –Validation (RMSECV), and Root Mean Square Error of Prediction (RMSEP), Bias and the coefficient of determination, R - squared (R^2).

3. Results and discussion

3.1. Comparison of milk and lactose spectroscopic signal

Lactose (β-D-Galactopyranosyl-(1 → 4)-D-glucose) is a disaccharide composed of glucose and galactose. In general, the NIR range is a combination of different overtones and different vibrations giving a more complex spectrum to interpret. Raman and MIR signals are comparable. However, observing the two plots in Fig. 1, it is clear that Raman spectra are more defined with stronger bands. The Raman spectrum of pure lactose is compared with that of milk in Fig. 1A; they are corrected by AsLS (range 1: (3600 - 2500 cm^{-1}) $p = 0.00001$, $\lambda = 10^4$, range 2: (2000 - 230 cm^{-1}) $p = 0.0001$, $\lambda = 10^4$ and 50 iterations for each). FT – IR spectra transformed in pseudo – absorbance and pre – processed using SNV are plotted in Fig. 1B.

Overall, bands at 4500–4200 cm^{-1} and 4300–4000 cm^{-1} are assigned to CH of aliphatic and aromatic groups, respectively. NH and OH stretching of ammines and alcohol overlap in the range 4000–3200 cm^{-1}. Usually, carbohydrates show a medium or strong O–H stretching vibration peak in 3520–3100 cm^{-1}(Socrates, 2001).

The lower wavenumber region, 3100–2800 cm^{-1}, comprising C–H stretching vibrations and for milk, involves both lipids and carbohydrates. The Raman lactose spectrum presents different peaks in this region (2979, 2919, 2904 and 2887 cm^{-1}). Only the milk spectrum shows signals between 2700 and 1600 cm^{-1}, 1746 cm^{-1} associated with C = O stretching for fatty acids and 1654 cm^{-1} combination of C = O stretching mode, CONH group, C = C stretching for amide I, proteins, and fatty acids respectively (Iñón et al., 2004; Martens et al., 2007). Furthermore, the range 1600–400 $cm^{-1}$is the most complicated having overlapped signals and including all the bending modes (Almeida et al., 2011). The range 1800 - 1400 cm^{-1} is relevant for all the studies that involve protein characterization in milk (Kher et al., 2007), however, lactose present peaks between 1500 and 1200 cm^{-1}(1470, 1457, 1415, 1358, 1339 and 1265 cm^{-1}) associated to deformational vibrations of HCH and CH_2OH groups (de Gelder et al., 2007; Yonzon et al., 2004). Part of the fingerprint region (1200–950 cm^{-1}) can be related to the vibrational modes of carbohydrates due to the contribution of C–C and C–O bonds; in fact, lactose has strong signals in this region in the Raman spectrum (1140, 1120, 1018 and 952 cm^{-1}) (Almeida et al., 2011; de Gelder et al., 2007; Iñón et al., 2004; Yonzon et al., 2004). Lactose has strong signals in the region between 1090 and 1030 cm^{-1} (1090, 1055 and 1039 cm^{-1})

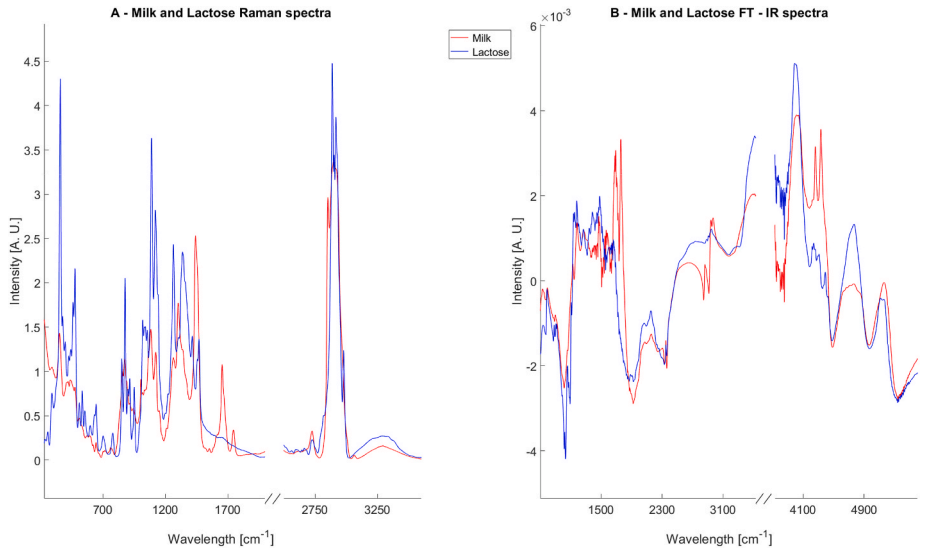

Fig. 1. Pure lactose and milk mean spectra. Plot A shows the mean Raman spectra. Each pixel spectrum was corrected by ALS (range 1: (3600 - 2500 cm-^{1}) p = 0.00001, λ = 10 ^{4}, range 2: (2000 - 230 cm-^{1}) p = 0.0001, λ = 10 ^{4} and 50 iterations for each) and the mean of 3 images was calculated. Plot B shows the mean FT - IR spectra of lactose and ilk. Each pixel was transforming in pseudo – absorbance and pre – processed using SNV and the mean of 3 images was calculated.

assigned to the C–O stretching vibrations (Socrates, 2001); in literature, this region has been used to quantify lactose in liquid milk (de Gelder et al., 2007; Li et al., 2015). The COH, CCH, OCH side groups deformation, and C–C stretching affect the 950-700 cm^{-1} region. This area is usually used to characterise the different anomeric forms (Mrozek & Weaver, 2002; Socrates, 2001; Yonzon et al., 2004). The Raman spectrum of lactose shows peaks in 916, 900, 878, 852, 779 and 742 cm^{-1}. All the peaks lower than 700 cm^{-1} (646, 633, 598, 555, 535, 512, 476,

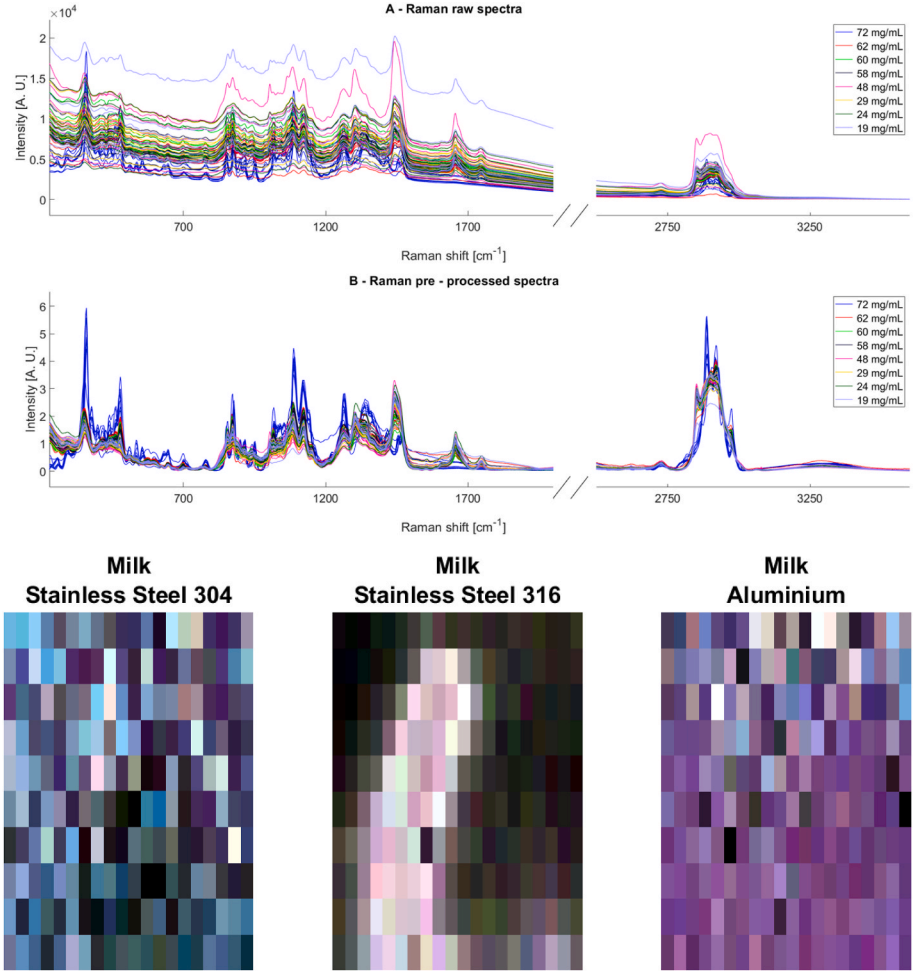

Fig. 2. Panel A shows the mean raw Raman spectra for all surfaces. Each pixel spectrum was corrected by ALS (range 1: (3600 - 2500 cm^{-1}) p = 0.00001, λ = 10^{4}, range 2: (2000 - 230 cm^{-1}) p = 0.0001, λ = 10 ^{4} and 50 iterations for each) and the mean was calculated and plotted in panel B. False RGB (Red, Green, and Blue) image built with values at R = 360 cm^{-1}, G = 476 cm^{-1} and B = 1339 cm^{-1} of pre – processed Raman spectra, they are rescaled between 0 and 1 and concatenated back.

461, 443, 428, 399, 378, 360 and 292 cm^{-1}) are related to skeletal signal, endocyclic and exocyclic deformation bands (Socrates, 2001).

3.1.1. Raman spectra and images

Raman spectra are sensitive to the presence of fluorescent molecules in the sample such as proteins. Fluorescence contributes to a baseline shift of the spectra. Another variability that can affect the baseline and noise in the spectra is due to the samples drying on different surfaces, i.e., aluminium, stainless steel 316 and 304.

Each Raman image covers an area of 1.90 × 0.90 mm with 200 spectra. In this study, each image was first corrected for cosmic peaks as previously described. Penalized Asymmetric Least Squares (AsLS) baseline removal was applied to remove the baseline fluorescence. This pre - processing was applied pixels wise: at each spectrum of the image. AsLS does not consider the nature and cause of the fluorescence, i.e., milk, lactose and/or metallic surface, however, it does remove the baseline without affecting the peak shape and position.

Fig. 1A in the *appendix* shows the raw and pre - processed data on stainless steel 304, stainless steel 316 and aluminium. The specific mean spectrum for each surface is plotted on the corresponding sample spectra for comparison. Even though it is evident that the surface signal can affect the spectra between 700 and 1700 cm^{-1}, it is not the only source of the baseline interference. Fluorescence has a strong influence in range 2 and it is evident in the baseline slope. This interference increases at lower lactose concentration. The baseline was removed efficiently by AsLS approach preserving the shapes and positions of the peaks (Fig. 2 – B).

The direct spectra interpretation is not simple due to the complexity of the milk matrix. However, the spectra produced in this study (Fig. 2 – B) show a common and clear decreasing trend related to lactose concentration. For all the surfaces the lactose variation is evident for the peaks lower than 700 cm^{-1} (related to skeletal signal, endocyclic and exocyclic deformation bands) (Socrates, 2001), around 1100 cm^{-1}, i.e., vibrational modes of carbohydrates due to the contribution of C–C and C–O bonds (Almeida et al., 2011; de Gelder et al., 2007; Iñón et al., 2004; Yonzon et al., 2004) and between 1500 and 1300 cm^{-1} associated to deformational vibrations of HCH and CH_2OH groups (de Gelder et al., 2007; Yonzon et al., 2004). This trend can be promising for the prediction of lactose concentration. In addition, similar interesting regions were found by Vaskova and Buckova (2016) comparing the signal of dried whole milk and lactose-free milk. They associated the range 400–600 cm^{-1} to endocyclic and exocyclic deformation, while the signal at 918 cm^{-1} and around 1070–1090 cm^{-1} to glucose with an intense signal at 1087 cm^{-1} being ascribed to C–O–H bending mode vibrations of lactose.

However, observing the false RGB (red, green, and blue) images of the milk samples on three metallic surfaces in Fig. 2 it is evident that the samples are not homogenous, and the lactose Raman signal is not constant over the entire samples. The false RGB images were built with values at R = 360 cm^{-1}, G = 476 cm^{-1} and B = 1339 cm^{-1} of pre – processed data, they are then rescaled between 0 and 1 and re-concatenated. Due to the non-homogeneity of the surfaces, the spectral imaging approach prevents biases that could arise due to selecting a specific area to collect the signal.

3.1.2. FT – IR spectra and images

FT – IR spectral images were collected simultaneously in the Near Infrared (NIR) and Mid Infrared (MIR) ranges covering the range 7500–475 cm^{-1}.300 spectra represent a spatial region of 3.00 × 2.25 mm were recorded in reflectance mode.

The spectrum of each pixel was firstly transformed in pseudo – absorbance, FT – NIR (5600 - 3730 cm^{-1}) and FT – MIR (3533–600 cm^{-1}) were treated independently, secondly, Standard Normal Variate (SNV) and Savitzy – Golay first derivative (SV1) were applied. Subsequently, the two ranges were re-concatenated after normalization of each block by division by their respective Frobenius' norm (total range: 5600–600 cm^{-1}). In the *appendix,* Fig. 3A shows the raw and corrected spectra per each surface. The mean spectrum of the corresponding metallic surface is plotted in black. A clear trend corresponding to increasing lactose concentration is evident in both, raw and pre – processed data in the entire range. Even though the SV1 is often applied to the Raman spectra to remove the baseline, the reasons for applying it on FT – IR spectra are different. The FT – IR spectra baseline can be affected by the surface material and the spatial irregularity; however, unlike Raman spectra, the atmosphere and the water vapour can also be detected. Therefore, it is necessary to work at two levels to optimise the spectral information: 1) removing noise and 2) removing the baseline offset. While the baseline can be removed without focusing on the cause, it is important to differentiate between the type of noise sources. Certainly, it is important to remove the signal due to the vapour water although the scattering due to surfaces or other molecules can be relevant to give an interpretation of the sample and detected. Therefore, it is necessary to work at two levels to optimise the spectral information: characterise the lactose concentration. The first step of SV1 is a simple smoothing, followed by the calculation of the first derivative which removes the baseline offset. However, the correction seems to be less efficient for spectra at a lower concentration, such as 19 mg/mL.

As for the Raman data, Fig. 3 shows the false RGB image (at Red = 2538 cm^{-1}, Green = 4048 cm^{-1} and Blue = 4763 cm^{-1}) of the milk samples. The spectra were pre – processed previously described.

As can be seen from the images, the distribution of the selected band intensities was not homogeneous, a classical point scan approach coupled with a sampling procedure could increase the prediction error. Even though the proposed approach is based on the mean of the samples, these spectra include the entire drop information.

3.2. PCA and Kennard-stone results

Three principal component analysis (PCA) models were calculated independently per modality (i.e., Raman, FT – MIR, FT – NIR). The three data sets were pre – processed as described before. The corrected spectra were centered on their mean before applying PCA algorithm.

3 PCs were selected for the Raman model to cover 96.92% explained variance. For more details, Fig. 4 panel A shows the scores plot for PC 1 which explains 46.72% variance, and PC 2 (45.65% explained variance). PC 2 separates the lactose standard from the milk samples while PC 1 separates the different lactose concentrations even though this separation is not very distinct. In addition, it seems that the different surfaces do not have a strong impact on the PCA results as there is no common trend between the similar surfaces. However, observing loadings in Fig. 4 – D, it is evident that, below 1440 cm^1, PC 2 loadings peaks overlap with that of the lactose spectrum in Fig. 1, while PC 1 does not seem to carry any specific lactose information; only the peak at 1440 cm^{-1} can be linked to lactose signal (de Gelder et al., 2007; Yonzon et al., 2004). So, this area affects more the separation between the different lactose concentration. Pre – processed FT – NIR and FT – MIR data were used to build two independent PCA models.

Five PCs were chosen to build the model in the MIR range explaining 94.14% of the original variance while four PCs were considered sufficient in the NIR range (96.05% explained variance). Both PC1, which explains 55.54% of the variance, and PC2, which covers 18.22% explained variance, separate the pure milk and lactose spectra from the samples with lactose variations (plot B in Fig. 4). The remaining concentrations are not clearly separated. The scores plot for the NIR range (plot C in Fig. 4) does not present any significant separation between the samples. Both scores plot for MIR and NIR ranges are not affected by the surface type.

In order to have the same calibration and test sets to compare the PLS models, the scores values were concatenated after being scaled by their respective Frobenius' norm. The Kennard – Stone algorithm was then applied to the obtained block to split the data into calibration and test sets. Calibration covers 70% of the data and the remaining 30% has been

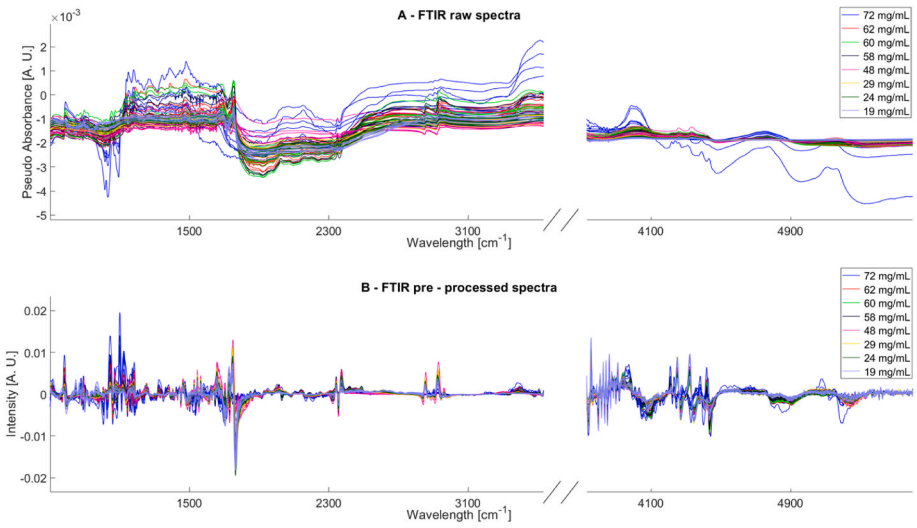

Fig. 3. Panel A shows the mean raw Ft - IR spectra. Each pixel spectrum was split in FT – NIR and FT – MIR range and pre – processed independently by SV1. The mean spectrum was calculated after concatenating back the two ranges normalised by their respective Frobenius' norm and plotted in panel B. False RGB (red, green, and blue) image built with values at R = 2538 cm^{-1}, G = 4048 cm^{-1} and B = 4763 cm^{-1} of pre – processed FT – IR spectra, they are rescaled between 0 and 1 and concatenated back.

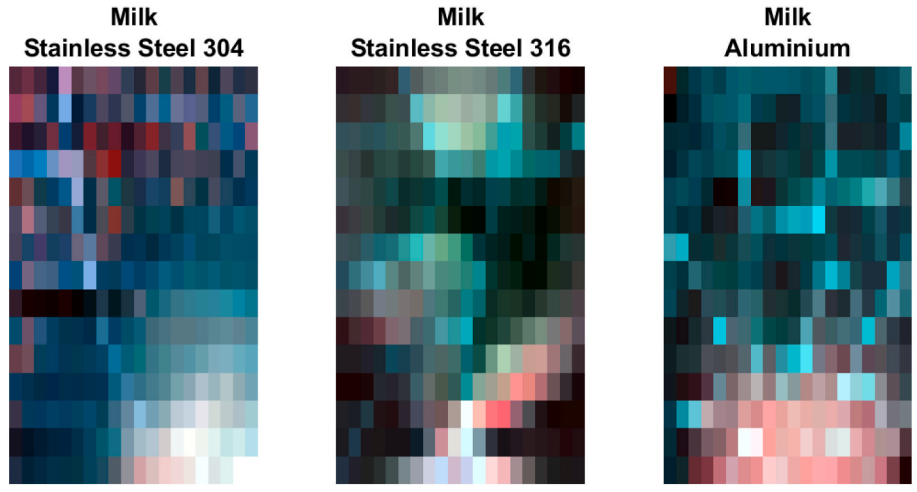

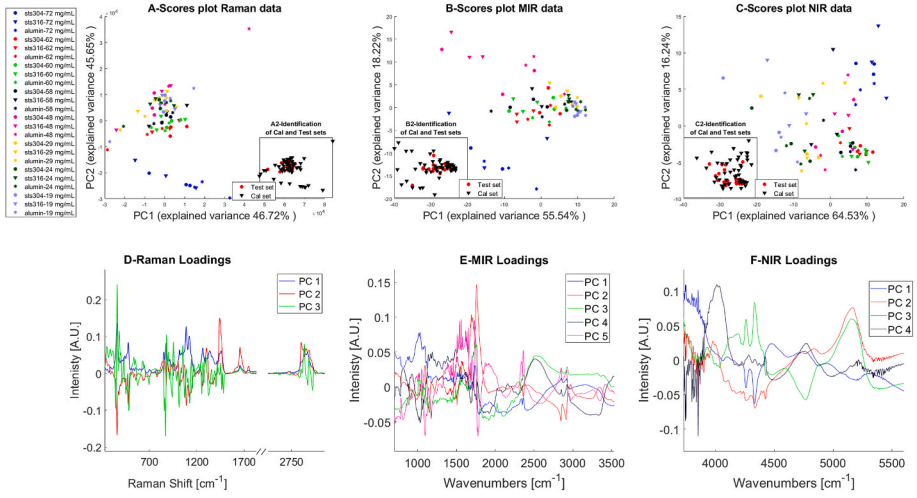

Fig. 4. PCA and Kennard - Stone results. Raman data: in panels A and D. Scores (A) plot PC 1 vs PC 2 and loadings (D) plots PC1, PC2, PC3. FT – MIR data: Scores (B) plot PC 1 vs PC 2 and loadings (E) plots PC1 – PC5. FT – NIR data: Scores (C) plot PC 1 vs PC 2 and loadings (F) plots PC1 – PC4. All PCA models were built using the mean image of corrected spectra. Scores values were concatenated after block scaling and were applied in the Kennard Stone algorithm to split the data set in calibration and training (A2 – B2 – C2).

identified as the test set. 21 samples were selected as the test set by the Kennard –Stone algorithm and are reported in table 1A in the appendix, while the remaining 51 samples were used as a training set to calibrate the PLS models. As it is possible to notice from the table, all the samples corresponding to pure lactose are included in the calibration set.

3.3. PLS results

The mean pre – processed spectra for each image were used to build the PLS model to predict the lactose concentration. The test set samples selected by the Kennard – Stone algorithm are reported in Table 1A. All

the other samples consist of the calibration set for EPO pre – processing and PLS modelling.

Different number of PCs (1–6) for EPO and nLVs (first 20) for PLS were examined to obtain the optimal prediction model using the calibration set. The best combination was selected using random cross – validation with 6 splits and 20 iterations, minimising the RMSECV over the first 20 LVs.

According to the approach described previously, the best model for the Raman data set was found at 5 PCs for EPO and 9 LVs. Fig. 2A in the *appendix* shows the EPO components removed during the pre – processing and the obtained pre – processed data.

In calibration and cross – validation, the model showed R^2 0.97 and 0.90 with 3.46 mg/mL and 6.35 mg/mL as RMSEC and RMSECV, respectively (BIAS Cal = 0 mg/mL and BIASCV = −0.28 mg/mL). Applying the obtained model to the test set, R^2 was 0.88 and RMSEP 7.73 mg/mL (BIASP = 3.42 mg/mL). Fig. 5 shows the real lactose concentration vs the predicted concentration and their residuals for this model. It is evident from the scatter plot that the major variability is at lower lactose concentrations, such as 24 and 19 mg/mL. The best performances are obtained using the entire range. Focusing on the range relevant for the carbohydrates functional group (900 - 1200 cm^{-1}) as suggested by Pinto et al. (2021) the model does not improve model performance (9 LVs R^2 0.92, 0.84 and 0.85 in training, cross – validation and test respectively). However, this range is included in the 417 variables obtained by analysing Variable Importance in Projection (VIP) from the full-range model. The new variables are selected considering only the variable with VIP scores greater than one. R^2 in training and cross-validation is 0.93 and 0.89 for 5 LVs (RMSEC = 4.78 mg/mL and RMSECV = 6.33 mg/mL) while during the test the R^2 is 0.86 (RMSEP = 7.47 mg/mL). These results are comparable with those of Mazurek et al. (2015). Focusing on bands at 370–860, 1020–1809 and 2800–2953 cm^{-1} and using laboratory mixtures to simulate milk as a training and validation sets, the R^2 in cross validation obtained by the authors of that study for carbohydrates prediction reached 0.811 for the highest spectral resolution tested (8 cm^{-1}). However, when the model was applied to real samples the $RSEP_{test}$ was 3.5–4.8%. Mazurek et al. (2015) report that the effect of water presence on the S/N for the Raman spectra is higher at 8 cm^{-1} resolution affecting the model prediction. In the present work, this interference has been removed experimentally using the single-drop dry milk technique.

The impact of micelles in liquid milk analysis has been demonstrated by Mohamed et al. (2021). In their study, protein, fat, lactose and total solids concentrations have been analysed in cow and camel liquid milk comparing results obtained by MIR and NIR spectroscopy. In particular, they found that the difference in the performances of models built in the two spectroscopic ranges for predicting the constituents was lower in the case of camel milk, ascribing these results to the different level of homogenization of two types of milk: the structure and dimension of casein micelles and fat globules in cow milk interference and scattering. On the other hand, the single-drop dry milk technique discussed in the present study significantly reduces the impact of these structures on the signals and, correspondingly, on the models built based on them.

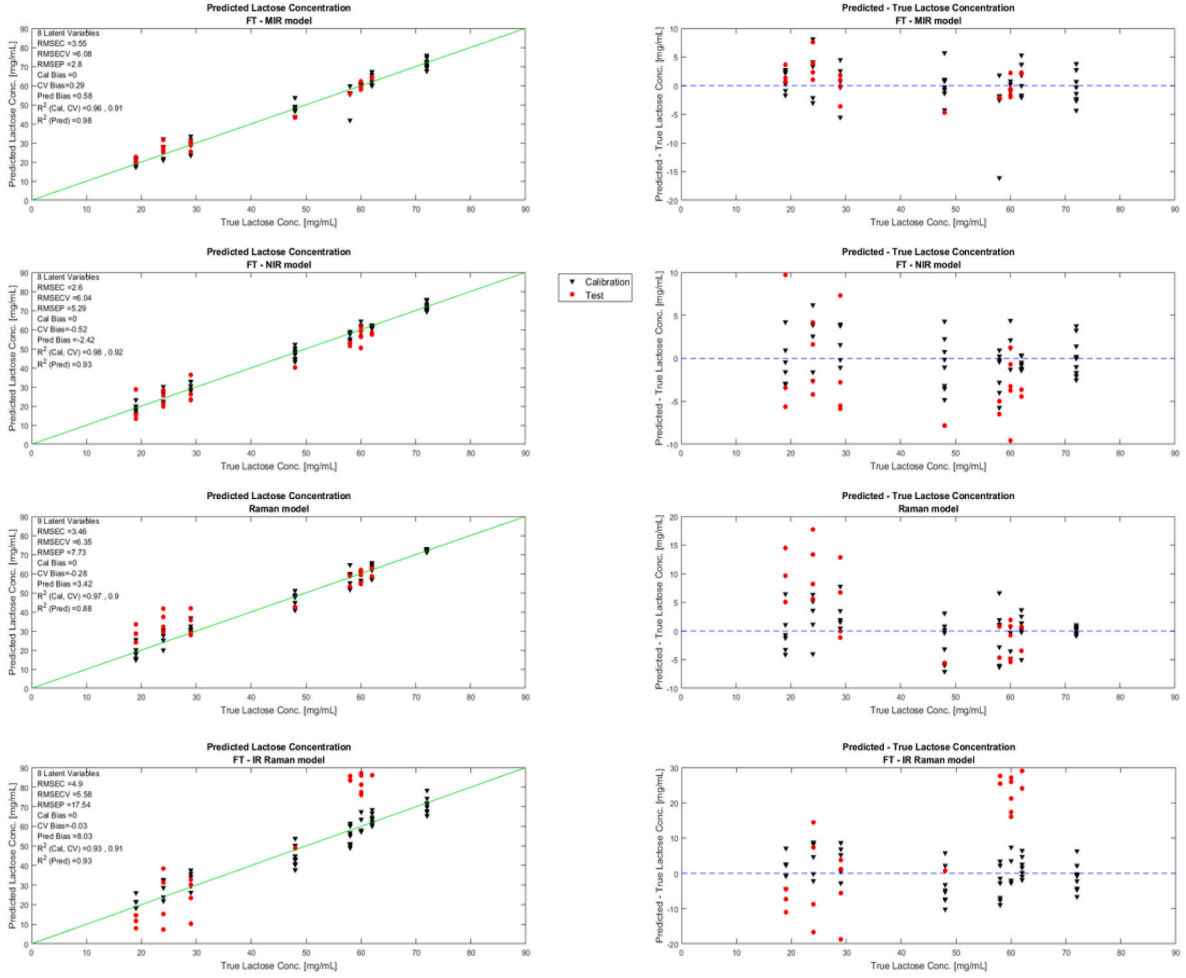

Fig. 5. Partial least squares regression (PLS) models built using mean centered pre – processed mean spectra. The actual lactose concentration vs predicted lactose concentration and residuals for prediction of lactose concentration are reported for the independent ranges and the fusion of all blocks. Black dots represent calibration set red dots is the test set.

The FT – MIR data set was corrected using 4 PCs for EPO while in the NIR range it was obtained using 5 PCs for EPO. Fig. 4A in the *appendix* shows the removed components by EPO and the obtained corrected spectra in both independent ranges.

The optimal model for the FT – MIR range was obtained using 8 LVs. In calibration and cross-validation, the model showed R^2 0.96 and 0.91 with 3.55 mg/mL and 6.08 mg/mL as RMSEC and RMSECV respectively (BIAS Cal = 0 mg/mL and BIASCV = 0.29 mg/mL). The results for the test set are $R^2 = 0.98$ and RMSEP = 2.80 mg/mL (BIASP = 0.58 mg/mL). The residuals and real lactose concentration vs the predicted concentration plots illustrate that an anomaly is evident at 58 mg/mL (Fig. 5). Similar performances were obtained by reducing the range to 346 variables by selecting the VIP scores greater than one. The optimal model, in this case, was obtained using 7 LVs, showing R^2 0.96 and 0.92 with 3.89 mg/mL and 5.83 mg/mL as RMSEC and RMSECV respectively. While R^2 and RMSEP are 0.96 and 3.71 mg/mL respectively for the test set. Both models using dried milk perform better than the similar analysis carried out on fresh milk obtained by Pinto et al. (2021) (R^2 0.96, 0.16 and 0.55 for training, cross-validation and test set respectively). However, the prediction performances decrease focusing on the 900 - 1200 cm^{-1} range (R^2 0.86, 0.66 and 0.93 for training, cross-validation and test set respectively). Similar trend is evident for the model in the NIR range (Fig. 5) The model that achieves better results in NIR range using 8 LVs, such as R^2 0.98 and 0.92 with 2.60 mg/mL and 6.04 mg/mL as RMSEC and RMSECV respectively (BIAS Cal = 0 mg/mL and BIASCV = -0.52 mg/mL) and in prediction $R^2 = 0.93$ and RMSEP = 5.29 mg/mL (BIASP = -2.42 mg/mL). Reducing the variables to 192 using the VIP scores, the optimal model is obtained using 4 LVs with R^2 0.97 and 0.91 with 4.28 mg/mL and 7.09 mg/mL as RMSEC and RMSECV respectively. While predicting the lactose in test set, the performances decrease to R^2 = 0.73 and RMSEP = 7.68 mg/mL.

In contrast to the Raman results, comparing the plots in Fig. 5, the prediction obtained with FT – MIR and FT- NIR data shows greater homogeneity. Both models perform better than the Raman, in terms of R^2 and error. These findings are also coherent with Mazurek et al. (2015) study. They confirmed the better ability of MIR (FTIR-ATR, using 800–1017, 1063–1634 and 1732–1760 cm^{-1} bands) than Raman to quantify carbohydrates and all the other macronutrients tested (i.e., fats, proteins and dry matter).

To minimise the error and integrate the information contained in the different ranges, the second step of this analysis was focused on the fusion of all the blocks. In the *appendix* (Fig. 5A*)*, the predictions obtained by the models built with the fusion between NIR and MIR ranges (FT- IR) and Raman with FT – MIR and Raman with FT – NIR are reported. The same approach used for the independent data set was followed, i.e., firstly calibration and validation sets were corrected by EPO as described previously for each block. Secondly, the blocks were fused together after being scaled by their respective Frobenius' norm and then independent PLS models were built. As it is possible to see in Fig. 5A, these models did not perform as well as all three ranges together shown in Fig. 5.

The optimal model for the total block (Raman, FT – MIR and FT – NIR) was obtained using 8 LVs. This model presents RMSEC = 4.9 mg/mL and RMSECV = 5.58 mg/mL, $R^2 = 0.93$ and 0.91 for respectively calibration and cross validation mode. $R^2 = 0.93$ and RMSEP = 17.54 mg/mL are obtained by applying the selected model to the pre -processed mean spectra of the test set.

It is evident from the residuals plot in Fig. 5 for the total range that this approach amplifies the differences between the calibration and test set at higher lactose concentration.

Results from this study indicate that there is an important difference between the tested techniques. The optimal PLS model based on Raman spectra was obtained by correcting the spectra with (EPO) (5 PCs) and using 9 LVs. The R^2 for the test set is $R^2 = 0.88$ (RMSEP = 7.73 mg/mL). The FT – IR gives a better prediction for the test set. In detail, looking at the results for the two ranges, it is evident that the MIR provides better prediction accuracy than the NIR. Models for FT – NIR (5600 - 3730 cm^{-1}) (EPO 4 PCs and 8 LVs), performs on the test set $R^2 = 0.93$ (RMSEP = 5.29 mg/mL), conversely the FT – MIR data set has $R^2 = 0.98$ (RMSEP = 2.8 mg/mL) using EPO PCs = 3 and 8 LVs.The block fusion did not increase the information represented by the models (R^2 is 0.93 and RMSEP = 17.54 mg/mL). However, among all the proposed methodologies, the FT – MIR approach is the most promising. The obtained PLS model is stable with good results in cross validation and test.

4. Conclusion

This study demonstrates that both FT- MIR and FT – NIR and Raman spectral imaging are promising techniques for the prediction of lactose concentration in dried whole milk without the use of additional standards. However, the three blocks together perform not well as all three ranges separately. In fact, the best prediction was obtained with FT – MIR data set $R^2 = 0.98$ (RMSEP = 2.8 mg/mL).

The FT – MIR in addition to giving a more stable model with lower prediction errors, represents the most relevant technique to be applied in real life, due to the lower cost of instrumentation and amenability to macroscopic spectral imaging.

CRediT authorship contribution statement

Vicky Caponigro: Conceptualization, Methodology, Formal analysis, Writing – original draft. **Federico Marini:** Conceptualization, Methodology, Formal analysis, Supervision, Writing – review & editing, Amalia Scannell, Conceptualization, Writing – review & editing, Funding acquisition. **Aoife A. Gowen:** Conceptualization, Methodology, Formal analysis, Supervision, Writing – review & editing, Funding acquisition.

Declaration of competing interest

The authors declare that they have no known competing financial interests or personal relationships that could have appeared to influence the work reported in this paper.

Data availability

Data will be made available on request.

Acknowledgement

This work was supported by Science Foundation Ireland (SFI) [Proposal ID 15/IA/2984—HyperMicroMacro].

Appendix A. Supplementary data

Supplementary data to this article can be found online at https://doi.org/10.1016/j.foodcont.2022.109351.

References

Almeida, M. R., Oliveira, K. D. S., Stephani, R., & de Oliveira, L. F. C. (2011). Fourier-transform Raman analysis of milk powder: A potential method for rapid quality screening. *Journal of Raman Spectroscopy, 42*(7), 1548–1552. https://doi.org/10.1002/jrs.2893

Alves da Rocha, R., Paiva, I. M., Anjos, V., Furtado, M. A. M., & Bell, M. J. V. (2015). Quantification of whey in fluid milk using confocal Raman microscopy and artificial neural network. *Journal of Dairy Science, 98*(6), 3559–3567. https://doi.org/10.3168/jds.2014-8548

Barnes, R. J., Dhanoa, M. S., & Lister, S. J. (1989). Standard normal variate transformation and de-trending of near-infrared diffuse reflectance spectra. *Applied Spectroscopy, 43*(5), 772–777. https://doi.org/10.1366/0003702894202201

Baskaran, S., & Sathiavelu, M. (2020). Application of Attenuated Total Reflection - Fourier Transform Infrared spectroscopy to characterize the degradation of littered multilayer food packaging plastics. *Vibrational Spectroscopy, 109*, Article 103105. https://doi.org/10.1016/j.vibspec.2020.103105

Biancolillo, A., Marini, F., Ruckebusch, C., & Vitale, R. (2020). Chemometric strategies for spectroscopy-based food authentication. *Applied Sciences, 10*(18), 6544. https://doi.org/10.3390/app10186544

Cattaneo, T. M. P., Cabassi, G., Profaizer, M., & Giangiacomo, R. (2009). Contribution of light scattering to near infrared absorption in milk. *Journal of Near Infrared Spectroscopy, 17*(6), 337–343. https://doi.org/10.1255/jnirs.867

Gambelli, L. (2017). Milk and its sugar-lactose: A picture of evaluation methodologies. *Beverages, 3*(4), 35. https://doi.org/10.3390/beverages3030035

de Gelder, J., de Gussem, K., Vandenabeele, P., & Moens, L. (2007). Reference database of Raman spectra of biological molecules. *Journal of Raman Spectroscopy, 38*(9), 1133–1147. https://doi.org/10.1002/jrs.1734

Gorla, G., Mestres, M., Boqué, R., Riu, J., Spanu, D., & Giussani, B. (2020). *ATR-MIR spectroscopy to predict commercial milk major components: A comparison between a handheld and a benchtop instrument.* Chemometrics and Intelligent Laboratory Systems. https://doi.org/10.1016/J.CHEMOLAB.2020.103995, 200.

Gowen, A. A., Pu, Y., & Caponigro, V. (2020). Spectral imaging for dairy products. In *Reference module in food science*. Elsevier. https://doi.org/10.1016/B978-0-12-818766-1.00116-1.

He, H., Sun, D.-W., Pu, H., Chen, L., & Lin, L. (2019). Applications of Raman spectroscopic techniques for quality and safety evaluation of milk: A review of recent developments. *Critical Reviews in Food Science and Nutrition, 59*(5), 770–793. https://doi.org/10.1080/10408398.2018.1528436

Holt, C., Carver, J. A., Ecroyd, H., & Thorn, D. C. (2013). Invited review: Caseins and the casein micelle: Their biological functions, structures, and behavior in foods1. *Journal of Dairy Science, 96*(10), 6127–6146. https://doi.org/10.3168/jds.2013-6831

Iñón, F. A., Garrigues, S., & de La Guardia, M. (2004). Nutritional parameters of commercially available milk samples by FTIR and chemometric techniques. *Analytica Chimica Acta, 513*(2), 401–412. https://doi.org/10.1016/j.aca.2004.03.014

Jollife, I. T., & Cadima, J. (2016). Principal component analysis: A review and recent developments. *Philosophical Transactions of the Royal Society A: Mathematical, Physical & Engineering Sciences, 374*(Issue 2065). https://doi.org/10.1098/rsta.2015.0202. Royal Society of London.

Kennard, R. W., & Stone, L. A. (1969). Computer aided design of experiments. *Technometrics, 11*(1), 137–148. https://doi.org/10.1080/00401706.1969.10490666

Kher, A., Udabage, P., McKinnon, I., McNaughton, D., & Augustin, M. A. (2007). FTIR investigation of spray-dried milk protein concentrate powders. *Vibrational Spectroscopy, 44*(Issue 2), 375–381. https://doi.org/10.1016/j.vibspec.2007.03.006

Li Vigni, M., Durante, C., Michelini, S., Nocetti, M., & Cocchi, M. (2020). Preliminary assessment of parmigiano reggiano authenticity by handheld Raman spectroscopy. *Foods, 9*(11), 1563. https://doi.org/10.3390/foods9111563

Li, M., Chen, J., Xu, J., Fu, S., & Gong, H. (2015). Determination of lactose in milk by Raman spectroscopy. *Analytical Letters, 48*(8), 1333–1340. https://doi.org/10.1080/00032719.2014.979358

Lynch, J. M., Barbano, D. M., Schweisthal, M., & Fleming, J. R. (2006). Precalibration evaluation procedures for mid-infrared milk analyzers. *Journal of Dairy Science, 89*(7), 2761–2774. https://doi.org/10.3168/jds.S0022-0302(06)72353-0

Martens, H., Kohler, A., Afseth, N., Wold, J., Harsleth, M., Berget, I., Ådnøy, T., Skaugen, M., Isaksson, T., Vegarud, G., Criscione, A., Mevik, B., Frøst, M., Randby, Å., Prestløkken, E., Berg, P., Kent, M., Lien, S., & Omholt, S. (2007). High-throughput measurements for functional genomics of milk. *Journal of Animal and Feed Sciences, 16*(Suppl. 1), 172–189. https://doi.org/10.22358/jafs/74190/2007

Mazurek, S., Szostak, R., Czaja, T., & Zachwieja, A. (2015). Analysis of milk by FT-Raman spectroscopy. *Talanta, 138*, 285–289. https://doi.org/10.1016/j.talanta.2015.03.024

McMahon, D. J., & Oommen, B. S. (2008). Supramolecular structure of the casein micelle. *Journal of Dairy Science, 91*(5), 1709–1721. https://doi.org/10.3168/JDS.2007-0819

Mohamed, H., Nagy, P., Agbaba, J., & Kamal-Eldin, A. (2021). Use of near and mid infrared spectroscopy for analysis of protein, fat, lactose and total solids in raw cow and camel milk. *Food Chemistry, 334*, Article 127436. https://doi.org/10.1016/j.foodchem.2020.127436

Mrozek, M. F., & Weaver, M. J. (2002). Detection and identification of aqueous saccharides by using surface-enhanced Raman spectroscopy. *Analytical Chemistry, 74*(16), 4069–4075. https://doi.org/10.1021/ac020115g

Pinto, P. A., Anconi, A. C. S. A., de Abreu, L. R., Magalhães, E. J., & Nunes, C. A. (2021). Strategies to determine lactose in cow milk by mid infrared spectroscopy. *Journal of Food Composition and Analysis, 104*, Article 104176. https://doi.org/10.1016/j.jfca.2021.104176

Piqueras, S., Duponchel, L., Tauler, R., & de Juan, A. (2014). Monitoring polymorphic transformations by using in situ Raman hyperspectral imaging and image multiset analysis. *Analytica Chimica Acta, 819*, 15–25. https://doi.org/10.1016/J.ACA.2014.02.027

Portnoy, M., & Barbano, D. M. (2021). Lactose: Use, measurement, and expression of results. *Journal of Dairy Science, 104*(7), 8314–8325. https://doi.org/10.3168/jds.2020-18706

Roger, J. M., Chauchard, F., & Bellon-Maurel, V. (2003). EPO-PLS external parameter orthogonalisation of PLS application to temperature-independent measurement of sugar content of intact fruits. *Chemometrics and Intelligent Laboratory Systems, 66*(2), 191–204. https://doi.org/10.1016/S0169-7439(03)00051-0

Savitzky, A., & Golay, M. J. E. (1964). Smoothing and differentiation of data by simplified least squares procedures. *Analytical Chemistry, 36*(8), 1627–1639. https://doi.org/10.1021/ac60214a047

Socrates, G. (2001). In *Infrared and Raman characteristic group frequencies. Tables and charts*. John Wiley and Sons, Ltd. Third.

Tan, Z., Lou, T. T., Huang, Z. X., Zong, J., Xu, K. X., Li, Q. F., & Chen, D. (2017). Single-drop Raman imaging exposes the trace contaminants in milk. *Journal of Agricultural and Food Chemistry, 65*(Issue 30). https://doi.org/10.1021/acs.jafc.7b01814

Taylan, O., Cebi, N., Tahsin Yilmaz, M., Sagdic, O., & Bakhsh, A. A. (2020). Detection of lard in butter using Raman spectroscopy combined with chemometrics. *Food Chemistry, 332*, Article 127344. https://doi.org/10.1016/j.foodchem.2020.127344

Valand, R., Tanna, S., Lawson, G., & Bengtström, L. (2020). A review of Fourier Transform Infrared (FTIR) spectroscopy used in food adulteration and authenticity investigations. In *Food additives and contaminants - Part A chemistry, analysis, control, exposure and risk assessment* (Vol. 37, pp. 19–38). Taylor and Francis Ltd. https://doi.org/10.1080/19440049.2019.1675909. Issue 1.

Vaskova, H., & Buckova, M. (2016). Measuring the lactose content in milk. *MATEC Web of Conferences, 76*, Article 05011. https://doi.org/10.1051/MATECCONF/20167605011

Wu, Z., Pu, H., & Sun, D. W. (2021). Fingerprinting and tagging detection of mycotoxins in agri-food products by surface-enhanced Raman spectroscopy: Principles and recent applications. In *, Vol. 110. Trends in food science and technology* (pp. 393–404). Elsevier Ltd. https://doi.org/10.1016/j.tifs.2021.02.013.

Yonzon, C. R., Haynes, C. L., Zhang, X., Walsh, J. T., & van Duyne, R. P. (2004). A glucose biosensor based on surface-enhanced Raman scattering: Improved partition layer, temporal stability, reversibility, and resistance to serum protein interference. *Analytical Chemistry, 76*(1), 78–85. https://doi.org/10.1021/ac035134k